ACS OMEGA

http://pubs.acs.org/journal/acsodf

Article

WS_2 Transistors with Sulfur Atoms Being Replaced at the Interface: First-Principles Quantum-Transport Study

Chih-Hung Chung, Hong-Ren Chen, Meng-Ju Ho, and Chiung-Yuan Lin*

Cite This: *ACS Omega* 2023, 8, 10419−10425

Read Online

ACCESS | Metrics & More | Article Recommendations

ABSTRACT: Reducing the contact resistance is one of the major challenges in developing transistors based on two-dimensional materials. In this study, we perform first-principles quantum-transport calculations by adopting a novel type of partially sulfur-replaced edge contact metal/WSX/WS_2 in order to lower the Schottky barrier height and in turn reduce the contact resistance. Here, the sulfur replacements produce a segment of the metamaterial WSX (X = P, As, F, and Cl), using group V or halogen atoms to substitute sulfur atoms on one side of a WS_2 monolayer. We further compare the effects of such sulfur replacements on the interface metallization and bonding. Such WSX-buffered contacts exhibit contact resistances as low as 142 and 173 Ω·μm for the p-type Pt/WSP/WS_2 and n-type Ti/WSCl/WS_2 edge contacts, respectively. Moreover, ab initio molecular dynamics is employed to observe a stable standalone WSX monolayer at room temperature.

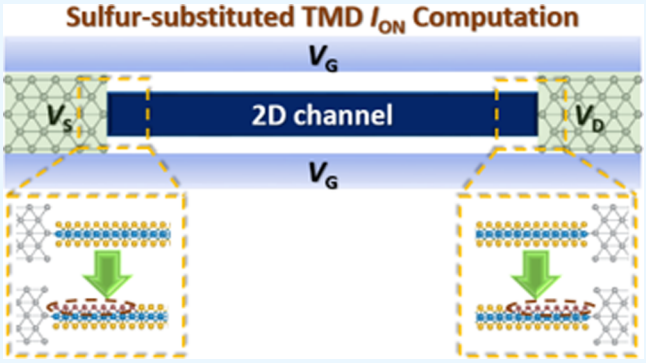

INTRODUCTION

Transition metal dichalcogenides (TMDs) are a series of two-dimensional (2D) materials with a wide band gap and high carrier mobility, usually denoted by MX_2, where M is the transition metal element and X is the chalcogen element, e.g., WS_2, MoS_2, $MoSe_2$, and WSe_2. When TMDs are used as channel materials for transistors, not only can the short channel effect be overcome and transistors be further miniaturized, but also a high on/off current ratio, carrier mobility, and thermal stability can be achieved.[1] However, the most pressing challenge in developing TMD-based field-effect transistors (FETs) is to reduce the contact resistance between metal and TMDs because TMDs do not have dangling bonds on the contact surface.[2,3]

In the TMD-based FETs, the contact geometry of metal and TMDs can typically be classified as top, edge, and combined contacts.[4] Several experiments have successfully produced edge contact structures.[5] Unlike the top contact having a van der Waals gap, in an edge contact, TMDs form a direct contact with the metal by bonding. Moreover, it is already demonstrated for the n-type contact that the covalent bond in the edge contact will result in a lower Schottky barrier height (SBH) than that of the top contact.[6] On the other hand, despite the fact that the n-type edge contact of atomistically thin TMDs can have a contact resistance as low as 630 Ω·μm,[7] the p-type contacts are rarely reported to exhibit satisfactorily low contact resistance.

Among the typical TMDs, WS_2 has its electron and hole mobilities not only close to each other in order of magnitude but also the highest[8] and is hence used as the channel material in this study. First-principles calculations are carried out to find the SBH of the WS_2 monolayer in contact with different metals,[9] indicating that Ti/WS_2 has the minimum electron SBH and Pt/WS_2 has the lowest hole SBH. However, even though one adopts Pt to be the lead, in reality, the contact may still suffer from the defect-induced Fermi-level pinning and consequently be unable to reach a satisfactorily low SBH.

For WS_2 FETs with different metal leads, it is not possible to obtain p- or n-type FETs with sufficiently low contact resistance (R_c) even if one chooses a metal of high or low work function.[10] Past studies on the contact resistance of bulk semiconductors show that interface doping can effectively reduce R_c.[11−13] A similar idea is extended to TMD contacts by piecewise replacing chalcogens with group V or halogen atoms near the interface, for example, doping of nitrogen,[14,15] fluorine,[16] phosphorus,[17] and chlorine.[18] Therefore, in this study, we generalize the ideas to replace an area of the sulfur

Received: December 30, 2022
Accepted: February 17, 2023
Published: March 8, 2023

atoms near the metal/WS_2 interface to form a local WSX (X = P, As for the p-type contacts; Cl, for the n-type contacts) segment at each end of WS_2, in the goal of further reducing the SBH over the conventional edge contacts.

COMPUTATIONAL DETAILS

In this study, we perform density functional theory (DFT) and nonequilibrium Green function[19] calculations as implemented in Vienna Ab initio Simulation Package (VASP)[20] and NanoDCAL.[21−23] The former and latter adopt the basis sets of the projector augmented wave and the linear combination of atomic orbitals, respectively. We also perform, for studying the stability of WSX, the ab initio molecular dynamics (MD) calculations using VASP with the canonical (NVT) ensemble.

Using DFT-LDA,[24,34] we obtain for the WS_2 channel and metal leads their bulk properties $a(WS_2)$ = 3.152 Å,[25] $E_g(WS_2)$ = 1.957 eV,[26] a(Ti) = 2.917 Å,[27] and a(Pt) = 3.910 Å,[28] which all agree excellently with the experiments.[25−29] Spin−orbit coupling (SOC)[24] is included in all our calculations throughout this study. Based on the improved electrostatics and higher drive current of double-gate MOSFETs,[30] we aim to adopt such a device structure in our study. Also, owing to the heavy computational cost required to perform the simulations on the large and realistic system, a reduced model is thus used for less computational expense. We start by constructing p- and n-type low-SBH edge contacts with Pt and Ti as the metal leads shown in Figure 1a,b, respectively. Each

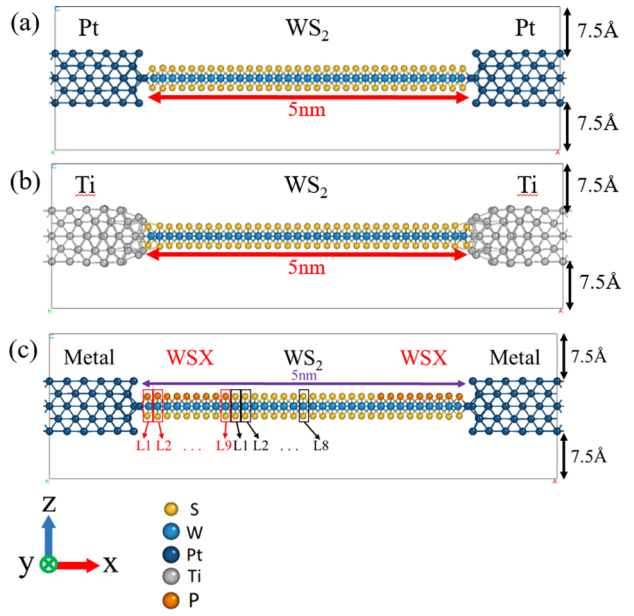

Figure 1. Atomistic structure of the two-lead model of the edge contact with a 5 nm 2D sheet. (a) Pt/WS_2. (b) Ti/WS_2. (c) Pt/WSP/WS_2 as an example to illustrate a general metal/WSX/WS_2 contact.

end of the lead is modeled as a five-atomic-layer slab aligned with the same normal direction of the monolayer WS_2. To minimize the lattice mismatch between the metal and TMD, we maintain minimum supercells of ×2 along the $[\bar{1}10]$ axis of the Pt(110) plane and ×1 along the WS_2 edge. Due to the residual small lattice mismatch based on the above supercells, we apply a 2.15% compression strain along the $[\bar{1}10]$ crystal axis of platinum and allow the other two perpendiculars to expand accordingly. Similarly, it is 4.17% in the case of Ti/WS_2 contacts. Such a conventional edge contact serves as the starting point to further construct the novel metal/WSX/WS_2, as shown in Figure 1c. We relax all the constructed contact structures using VASP until the forces of the interface atoms reach below 0.05 eV/Å. As a quick examination of the stability of the above WSX segment, we perform ab initio MD of a standalone WSX monolayer at 300 K, with a 1 fs time step and a total simulation time of 10 ps.

The simplest quantum-transport calculation is conventionally done in a two-lead model, as shown in Figure 1. To further enable the gate control of a two-lead contact system, we introduce the top and bottom gates as equipotential boundaries, located 7.5 Å above and below the slabs of the metal leads. To quantify the gating effect, we define the gating potential energy to be atomistic potential energy with a nonzero V_G subtracted by the zero-gating one. We plot this gating potential energy with the drain-to-source voltage V_{DS} = 50 mV and the gate voltage V_G = −5 V in Figure 2. Because the

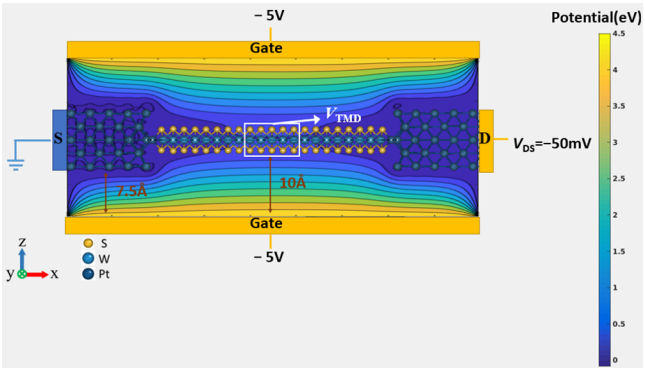

Figure 2. Gating potential energy contour of the Pt/WS2 edge contact system with the source terminal being grounded. Its average at the middle TMD, V_{TMD}, is defined in the region indicated by the white empty box.

gating effect specifically at the piece of TMD actually determines how the channel is affected by the gate voltage, we define V_{TMD} as the average gating potential energy within the TMD segment in the middle that is sufficiently away from the interface to restore the band diagram of a standalone TMD.

RESULTS AND DISCUSSION

The WSX segment is a metamaterial that has not been studied before; yet its stability is the first thing that needs to be inspected. We perform ab initio MD of a standalone WSX monolayer at 300 K. For each particular sulfur substitute, the MD of the WSX monolayer spans the simulation time of 10 ps. We take the snapshot structures of all five WSX monolayers at t = 0, 5000, and 10,000 fs. As can be seen in Figure 3, only WSF is severely deformed and is hence the only unstable monolayer. From this point, we will concentrate on the other four stable ones in studying the sulfur-replaced contacts.

Each left half figure among Figure 4a−e shows the band diagram at V_G = 0, where the p-type contacts with Pt leads all have their Fermi level (E_F) closer to their valence band edges (VBE), as shown in Figure 4a−c , while the n-type contacts with Ti leads induce E_F to approach conduction band edges (CBE), as displayed in Figure 4d,e. If we compare Pt/WS_2 and Pt/WSX/WS_2 (Ti/WS^2 and Ti/WSX/WS_2), we find that interface sulfur replacements significantly bring VBE (CBE)

https://doi.org/10.1021/acsomega.2c08275
ACS Omega 2023, 8, 10419−10425

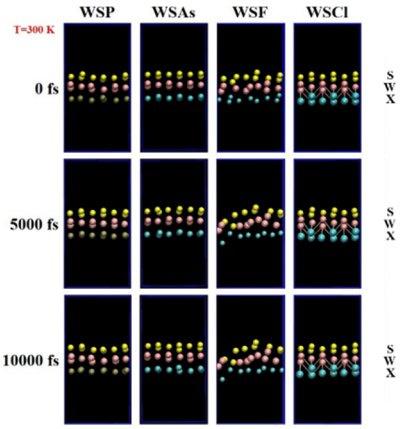

Figure 3. Simulated ab initio MD of the WSX (X = P, As, F, and Cl). In each snapshot, from the top layer to the bottom are sulfur, tungsten, and phosphorous or arsenic atoms, respectively.

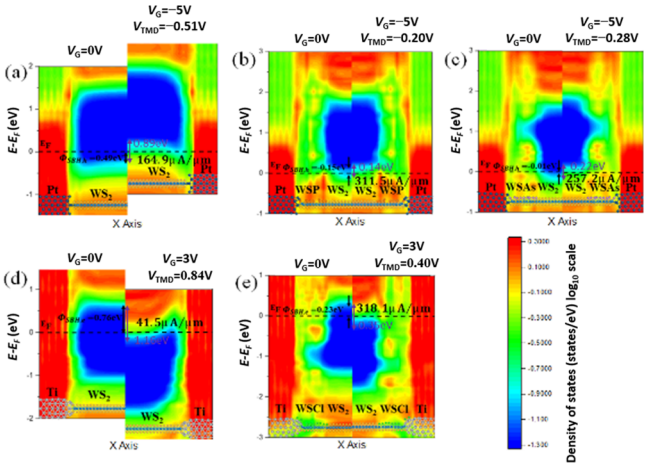

Figure 4. LDDOS of the edge contacts with a 5 nm long 2D sheet before and after applying V_G and V_{DS}. The corresponding SBH, denoted as Φ_{SBH}, and the on-state calculated current are also shown in each figure. (a) Pt/WS_2. (b) Pt/WSP/WS_2. (c) Pt/WSAs/WS_2, where the residual length of WS_2 is 2.5 nm for the latter two. (d) Ti/WS_2. (e) Ti/WSCl/WS_2.

much closer to E_F in a p-type (n-type) contact and are hence expected to lower the contact resistance even by only looking at those V_G = 0 band diagrams revealed by local device density of states (LDDOS). When the gate voltage is switched on to −5 and 3 V on the p- and n-type contacts, respectively, we observe that all the band shifts follow a highly consistent trend with V_{TMD}. Such a V_G-induced band shift of TMD affects the entire band diagram of the simple edge contact differently from that of the WSX type. Under V_G = −5 V, the simple Pt/WS_2 has a non-negligible VBE bending, while the partially sulfur-replaced Pt/WSP/WS_2 and Pt/WSAs/WS_2 turn VBE into a flat one. The corresponding V_{DS} = 50 mV currents calculated by quantum transport show that the currents of Pt/WSP/WS_2 and Pt/WSAs/WS_2 increase from Pt/WS_2 by more than 50%, which consistently reflects the flattened band bending due to sulfur replacements by group V atoms. As to the n-type contacts, when the Ti/WS_2 edge contact undergoes interface sulfur replacements by halogens, the current at V_G = 3 V and V_{DS} = 50 mV drastically increases by nearly eight times from Ti/WS_2 to Ti/WCl/WS_2, as a consequence of the flattened band bending in Ti/WSCl/WS_2.

Next, we revisit the atomistic structures in Figure 1 and expect the metal-TMD interface bonding exists whether or not the sulfur replacement is performed. In addition, as we have observed in the band diagrams of Figure 4a,d, the metallization occurs near the metal/WS_2 interfaces and the subsequent band-bending profiles change to be flat towards the WS_2; however, near the WSX/WS_2 interfaces, the lengths of the metallization and band-bending regions have simultaneously shrunk to be negligible, as shown in Figure 4b,c,e. In summary, these results suggest that the TMD contact may in general contain the metal−TMD interface bonding, metallized TMD, band-bending gapped TMD, where beyond this contact region are the electronic structures of the bulk metal and standalone TMD. The abovementioned contact subregions are a few nanometers long along the channel length. In order to investigate such decomposed contact subregions, we build the simple edge contacts of Pt/WS_2 and Ti/WS_2 with WS_2 lengths of 1, 4, 5, and 6 nm, with the latter three channel lengths at an applied gate voltage but 1 nm ungated. Their calculated LDDOS are shown in Figure 5a,b. The contacts of 1

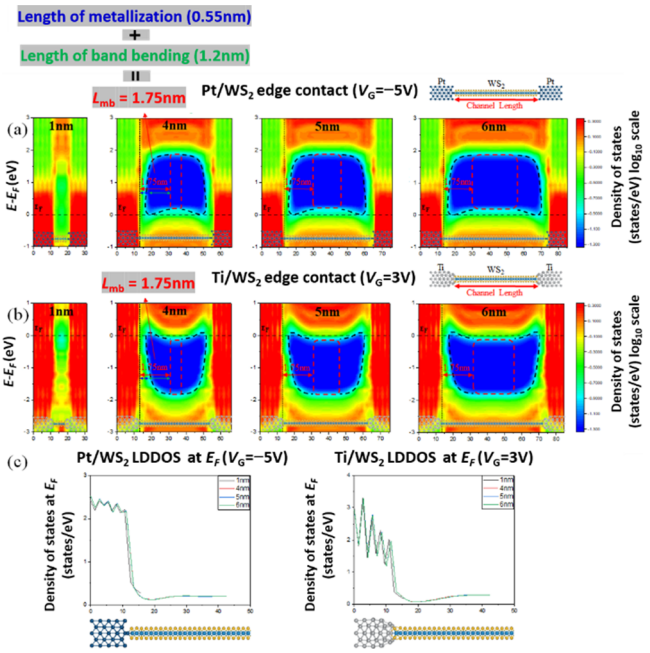

Figure 5. (a) Under V_G = −5 V, Pt/WS_2 LDDOS with channel lengths of 1, 4, 5, and 6 nm. (b) Under V_G = 3 V, Ti/WS_2 LDDOS with channel lengths of 1, 4, 5, and 6 nm. (c) LDDOS at E_F of the Pt/WS_2 and Ti/WS_2, plotted by matching the contact interfaces of different channel lengths, respectively.

nm WS_2 contain no gapped region, i.e., a fully metallized WS_2 sheet. As we continue to inspect the band diagrams of contacts with 4, 5, and 6 nm WS_2, we find their band profiles within a contact region independent of the channel length, as indicated in the region outside the red dashed boxes in Figure 5a,b. The length of either the metallization or band-bending (gap) region is found to be the same not only for varying channel lengths but also for different lead metals. These two lengths of the metal/WS_2 edge contact are 0.55 and 1.2 nm at each end, respectively, which sum up to 3.5 nm by counting both ends. Apparently, only the flat band diagram in the middle TMD increases with the channel length. We further quantitatively verify that the interface electronic structures, metallization, and

https://doi.org/10.1021/acsomega.2c08275
ACS Omega 2023, 8, 10419−10425

band bending are the same for different channel lengths, by comparing in Figure 5c the corresponding LDDOS at the gated E_F. The above observation makes one confident in using the transfer length method (TLM) to extract the contact resistance (R_c) from the calculated metal/TMD resistance versus channel length, as long as the TMD length is beyond the length of metallization plus band bending, denoted as L_{mb} (for metal/WS_2, L_{mb} = 3.5 nm). Also, in this case, such observed contact subregions suggest that the contact resistance can be decomposed into their individual contribution as

$$R_c = R_{im} + R_{bd} \quad (1)$$

where R_{im} is the resistance contributed by both the metal/WS_2 interface bonding and the metallized WS_2 segment, and R_{bd} is contributed by the band-bending region.

When turning ourselves to metal/WSX/WS_2, we first notice that in Figure 4b,c, the current of Pt/WSP/WS_2 is 20% more than that of Pt/WSAs/WS_2, and hence we will concentrate on solely the former from this point. We build such sulfur-replaced contacts with 2.5, 3.4, and 4.4 nm WS_2 lengths and keep the WSX segment 1.3 nm long at each end. Their calculated LDDOS are shown in Figure 6a,b. The metallization

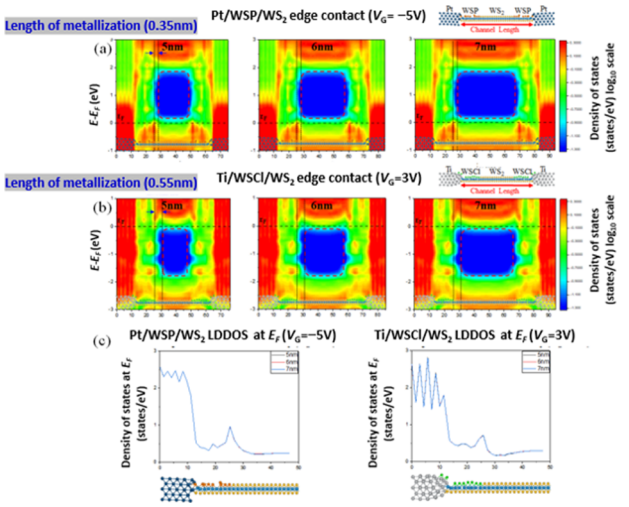

Figure 6. (a) Under V_G = −5 V, Pt/WSP/WS_2 LDDOS with channel lengths of 5, 6, and 7 nm. (b) Under V_G = 3 V, Ti/WSCl/WS_2 LDDOS with channel lengths of 5, 6, and 7 nm. (c) LDDOS at E_F of the Pt/WSP/WS_2 and Ti/WSCl/WS_2, plotted by matching the contact interfaces of different channel lengths, respectively.

of the simple edge contacts suggests that we pay attention to the few layers of WS_2 at its interface to the WSX. We find that within nine layers, there are metallicity-induced gap states (MIGS) with energy-dependent decay tails from the atomistic WSX/WS_2 interface toward the WS_2 side. For each particular contact, each MIGS tail terminates at a particular layer of WS_2. The collection of the termination within the energy gap window forms a vertically oriented $x(E)$ band-diagram curve, in contrast to the horizontally oriented $E(x)$ curves of VBE and CBE. Such $x(E)$ example curves can be visualized in Figure 5a,b and are also displayed in Figure 6a,b. In the simple edge contacts mentioned previously, such an $x(E)$ function and its curve reduce to a constant and vertical line section. The gap region of a WSX-type contact has not only the CBE and VBE as upper and lower boundaries, respectively, but also vertically oriented $x(E)$ as its non-trivial boundaries on the two sides. The x position where the band gap starts to fully open is located at the most right (left) position of the above left-side (right-side) boundary $x(E)$ and can also be considered as the termination position of the metallicity-induced gap band. MIGS partially fill the bandgap energy window of the WS_2 segment from the atomistic interface to this termination position, where this segment is called the MIGS decay length. When we inspect the band edges of the WSX-type contacts, we find that they have essentially no band bending, in contrast to the simple edge contacts. To this point, we are able to generalize eq 1 to be valid for both the simple edge and the WSX-type contacts. We achieve this by redefining R_{im} to be the resistance contributed by bonding of both the metal/WSP and WSP/WS_2 interfaces and the WS_2 segment within the MIGS decay length. (Note that this length reduces to the metallization length for a simple edge contact.) The meaning of R_{bd} remains unchanged as long as one keeps in mind R_{bd} = 0 for WSX-type contacts due to no band bending. The notation L_{mb} also remains valid by being redefined as the MIGS decay length plus the "zero band bending length". The metal/WSP/WS_2 contacts have $2L_{mb}$ = 0.7 nm, where the factor of 2 comes from counting both ends. Similar to the simple edge contacts, by inspecting Figure 6c, we are convinced that R_c indeed does not depend on the channel lengths, i.e., the TLM is also valid for the WSX types.

The LDDOS along the channel length provides information of metallization and band bending. Besides these two interface properties, R_c can also in general be contributed from the interface bonding, that is, the bonds between the atoms from different materials. Because the LDDOS along the channel length is obtained by averaging the local density of states per unit volume over the other two dimensions (channel width and perpendicular), it can hardly reveal the directionality of the 3D bonding clouds. Here, we adopt two approaches to study the interface bonding: one is the usual electron localization function (ELF),[31] and the other is the simultaneous plots of projected density of states (PDOS) of the two bonding atoms, which are spatially and energy resolved, respectively, and the latter will be called bonding PDOS for simplicity. We compare the interface bonding of the Pt/WS_2 and Pt/WSP/WS_2 contacts using the abovementioned two analysis tools. Both contacts mainly have covalent bonds at the interface with the Pt lead. As the Pt lead forms a p-type contact with WS_2, the band diagrams of V_G = −5 V in Figure 7a suggest that the band states which dominate the current transport lie within the energy range of 0.5 eV below VBE. That is, −1 to −0.5 eV in all the V_G = 0, bonding PDOS plots, as can be seen from the W−S bonding PDOS within WS_2. The bonding PDOS provides an idea of how many bonding states participate in the current transport. We compare the bonding PDOS before (Figure 7a) and after (Figure 7b) the phosphorous substitution at two interface locations Pt/WSP and WSP/WS_2. We find that at the Pt/WSP location, the after-substitution Pt−P and Pt−S bonds contain more transport-effective band states than the before-substitution Pt−S. Likewise, at WSP/WS_2, the W−P and W−S bonds contain more transport-effective band states than W−S of a WS_2 monolayer. Consequently, the Pt/WSP/WS_2 contact has its current transport across the interface bonds enhanced locally over the Pt/WS_2 simple edge contact.

In the previous paragraph, it is justified that R_c indeed does not depend on the channel lengths for both simple edge contacts and WSX type. We have already found out that in the presence of the interface WSP, an edge contact can have its

https://doi.org/10.1021/acsomega.2c08275
ACS Omega 2023, 8, 10419−10425

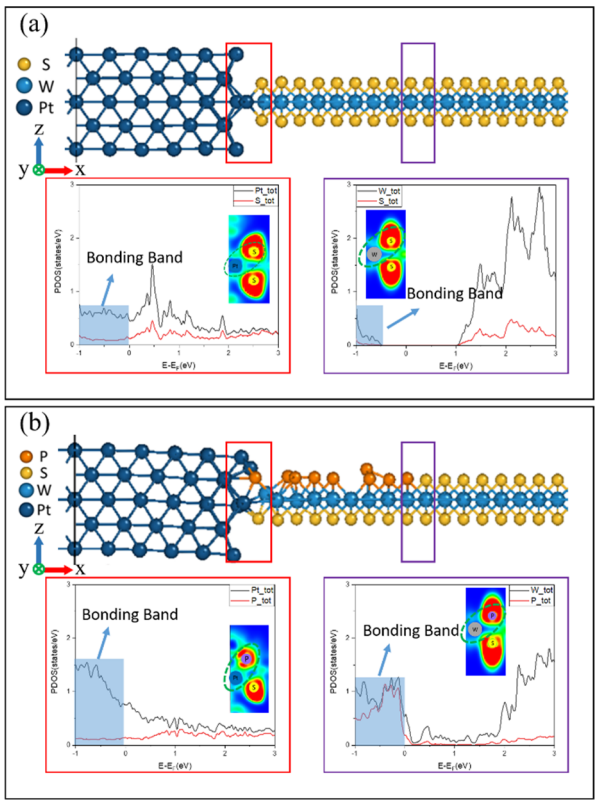

Figure 7. ELF and its corresponding PDOS of whose atoms form the bond of interest. The red and purple empty boxes specify the interface locations Pt/WSP and WSP/WS_2, respectively. (a) Pt/WS_2 edge contact. (b) Pt/WSP/WS_2 edge contact.

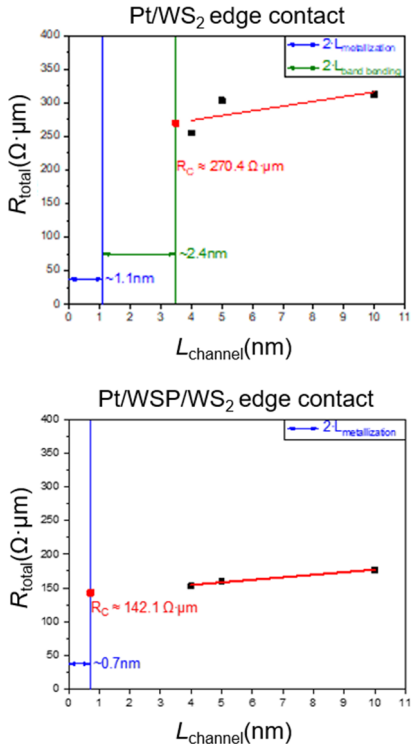

Figure 8. Plots of the system resistance vs the length of the WS_2 monolayer for the TLM. The systems refer to the following modeled contact structures of varying channel lengths: upper—Pt/WS_2 and lower—Pt/WSP/WS_2.

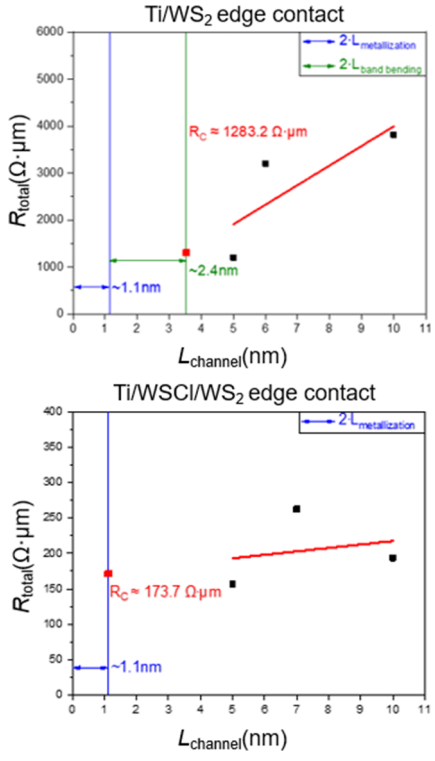

Figure 9. Plots of the system resistance vs the length of the WS_2 monolayer for TLM. The systems refer to the following modeled contact structures of varying channel lengths: upper—Ti/WS_2 and lower—Ti/WSCl/WS_2.

current enhanced by more than 50% as in Figure 4. In order to further obtain R_c, we achieve this by using the TLM, i.e., plotting the calculated system resistance of our contact model as a function of the channel length. We plot in Figure 8 the system resistance R of our modeled contact vs the length L of the WS_2 sheet. The estimated value $R_{sh} \approx 4\ \Omega{\cdot}\mu m$ is of course much smaller than the recently found experimental sheet resistance,[32] given the fact that our modeled contacts do not include electron−phonon scattering as well as any defect. Such relatively small R_{sh} make R_c dominate the system resistance. Moreover, as observed in the band diagrams of Figures 5 and 6, the sheet resistance is contributed microscopically from the middle WS_2 segment having a flat band along the channel length. As a result, the transmission line (system resistance vs channel length) should be interpolated at $L_{channel} = 2L_{mb}$ rather than the conventional $L_{channel} = 0$ in macro- or mesoscopic experiments ($L_{mb} \ll$ channel length). We recall that Pt/WS_2 and Pt/WSP/WS_2 have $2L_{mb}$ = 3.5 and 0.7 nm, respectively. As interpolated from Figure 8, a Pt/WSP/WS_2 contact has an R_c value that is half that of the Pt/WS_2, reaching below 150 $\Omega{\cdot}\mu m$. Besides that, from Figure 9, we also observe that n-type Ti/WSCl/WS_2 shows a steep decrease of R_c by nearly 90%, reaching as low as 173 $\Omega{\cdot}\mu m$.

The group V semi-metal Bi has been proven to effectively suppress the CB-contributed MIGS and thus achieve excellent ohmic contacts at the Bi/MoS_2 interface,[33] while we utilize the semi-metallic metamaterials formed by a TMD with chalcogens replaced by group V elements to demonstrate a negligible Schottky barrier for a p- and n-type contact.

https://doi.org/10.1021/acsomega.2c08275
ACS Omega 2023, 8, 10419−10425

CONCLUSIONS

By replacing the sulfur atoms of WS_2 with group V atoms near its interface with p-type leads such as Pt, we find that such a sulfur-replaced segment WSX exhibits the properties of a semi-metallic nanosheet. This WSX segment, buffered in between a TMD and a metal, significantly suppresses the MIGS of the TMD/metal direct contact, consequently reducing band bending. We explicitly calculate the contact resistance w/wo the semi-metallic buffer in the framework of first-principles quantum transport and find that R_c improved from nearly 300 $\Omega\cdot\mu$m to below 150 $\Omega\cdot\mu$m for the p-type contacts while seven times lower than that of the conventional n-type counterpart. The present study provides a potential alternative to lower R_c by introducing a semi-metallic sulfur-replaced nanosheet. The results should sparkle further experimental study and pave the way for applications in electronic devices.

AUTHOR INFORMATION

Corresponding Author

Chiung-Yuan Lin − *Department of Electronics and Electrical Engineering and Institute of Electronics, National Yang Ming Chiao Tung University, Hsinchu 300, Taiwan*; Email: genelin@nycu.edu.tw

Authors

Chih-Hung Chung − *Department of Electronics and Electrical Engineering and Institute of Electronics, National Yang Ming Chiao Tung University, Hsinchu 300, Taiwan*; orcid.org/0000-0003-3792-7427

Hong-Ren Chen − *Department of Electronics and Electrical Engineering and Institute of Electronics, National Yang Ming Chiao Tung University, Hsinchu 300, Taiwan*

Meng-Ju Ho − *Department of Electronics and Electrical Engineering and Institute of Electronics, National Yang Ming Chiao Tung University, Hsinchu 300, Taiwan*

Complete contact information is available at: https://pubs.acs.org/10.1021/acsomega.2c08275

Notes

The authors declare no competing financial interest.

ACKNOWLEDGMENTS

This work was financially supported by the "Center for the Semiconductor Technology Research" from the Featured Areas Research Center Program within the framework of the Higher Education Sprout Project by the Ministry of Education (MOE) in Taiwan. This work was also supported in part by the National Science and Technology Council, Taiwan, under Grant No. NSTC 111-2634-F-A49-008 and NSTC 111-2119-M-A49-005-MBK. We would like to thank Uni-edit (www.uni-edit.net) for editing and proof-reading this manuscript.

REFERENCES

(1) Li, L.; Yu, Y.; Ye, G. J.; Ge, Q.; Ou, X.; Wu, H.; Feng, D.; Chen, X. H.; Zhang, Y. Black phosphorus field-effect transistors. *Nanotechnology* **2014**, *9*, 372−377.

(2) Chang, H.-Y.; Zhu, W.; Akinwande, D. On the mobility and contact resistance evaluation for transistors based on MoS2or two-dimensional semiconducting atomic crystals. *Appl. Phys. Lett.* **2014**, *104*, 113504.

(3) Das, S.; Chen, H. Y.; Penumatcha, A. V.; Appenzeller, J. High performance multilayer MoS_2 transistors with scandium contacts. *Nano Lett.* **2013**, *13*, 100−105.

(4) Kang, J.; Liu, W.; Sarkar, D.; Jena, D.; Banerjee, K. Computational Study of Metal Contacts to Monolayer Transition-Metal Dichalcogenide Semiconductors. *Phys. Rev. X* **2014**, *4*, No. 031005.

(5) Li, R.; Cheng, Y.; Huang, W. Recent Progress of Janus 2D Transition Metal Chalcogenides: From Theory to Experiments. *Small* **2018**, *14*, No. e1802091.

(6) Bai, H.-F.; Xu, L.-C.; Di, M.-Y.; Hao, L.-Y.; Yang, Z.; Liu, R. P.; Li, X. Y. The intrinsic interface properties of the top and edge 1T/2H MoS_2 contact: A first-principles study. *J. Appl. Phys.* **2018**, *123*, No. 095301.

(7) Cai, F.; Deng, G.; Li, X.; Lin, F. Contact Resistance Parallel Model for Edge-Contacted 2D Material Back-Gate FET. *Electronics* **2020**, *9*, 2110.

(8) Jin, Z.; Li, X.; Mullen, J. T.; Kim, K. W. Intrinsic transport properties of electrons and holes in monolayer transition-metal dichalcogenides. *Phys. Rev. B* **2014**, *90*, No. 045422.

(9) Tang, H.; Shi, B.; Pan, Y.; Li, J.; Zhang, X.; Yan, J.; Liu, S.; Yang, J.; Xu, L.; Yang, J.; Wu, M.; Lu, J. Schottky Contact in Monolayer WS_2 Field-Effect Transistors. *Adv. Theory Simul.* **2019**, *2*, No. 1900001.

(10) Sik Hwang, W.; Remskar, M.; Yan, R.; Protasenko, V.; Tahy, K.; Doo Chae, S.; Zhao, P.; Konar, A.; Xing, H.; Seabaugh, A.; Jena, D. Transistors with chemically synthesized layered semiconductor WS_2 exhibiting 10^5 room temperature modulation and ambipolar behavior. *Appl. Phys. Lett.* **2012**, *101*, No. 013107.

(11) Guo, Y.; An, X.; Huang, R.; Fan, C.; Zhang, X. Tuning of the Schottky barrier height in NiGe/n-Ge using ion-implantation after germanidation technique. *Appl. Phys. Lett.* **2010**, *96*, 143502.

(12) Lin, H.-C.; Lin, C.-Y.; Shih, C.-J.; Tsui, B.-Y. First-principles calculations on the Schottky barrier height of the NiGe---N-type Ge contact with dopant segregation. In *International Symposium on Next-Generation Electronics*; IEEE, 2014.

(13) Zhao, Q. T.; Breuer, U.; Rije, E.; Lenk, S.; Mantl, S. Tuning of NiSi/Si Schottky barrier heights by sulfur segregation during Ni silicidation. *Appl. Phys. Lett.* **2005**, *86*, No. 062108.

(14) Azcatl, A.; Qin, X.; Prakash, A.; Zhang, C.; Cheng, L.; Wang, Q.; Lu, N.; Kim, M. J.; Kim, J.; Cho, K.; Addou, R.; Hinkle, C. L.; Appenzeller, J.; Wallace, R. M. Covalent Nitrogen Doping and Compressive Strain in MoS_2 by Remote N_2 Plasma Exposure. *Nano Lett.* **2016**, *16*, 5437−5443.

(15) Tang, B.; Yu, Z. G.; Huang, L.; Chai, J.; Wong, S. L.; Deng, J.; Yang, W.; Gong, H.; Wang, S.; Ang, K. W.; Zhang, Y. W.; Chi, D. Direct n- to p-Type Channel Conversion in Monolayer/Few-Layer WS_2 Field-Effect Transistors by Atomic Nitrogen Treatment. *ACS Nano* **2018**, *12*, 2506−2513.

(16) Chen, M.; Nam, H.; Wi, S.; Ji, L.; Ren, X.; Bian, L.; Lu, S.; Liang, X. Stable few-layer MoS_2 rectifying diodes formed by plasma-assisted doping. *Appl. Phys. Lett.* **2013**, *103*, 142110.

(17) Nipane, A.; Karmakar, D.; Kaushik, N.; Karande, S.; Lodha, S. Few-Layer MoS_2 p-Type Devices Enabled by Selective Doping Using Low Energy Phosphorus Implantation. *ACS Nano* **2016**, *10*, 2128−2137.

(18) Yang, L.; Majumdar, K.; Liu, H.; Du, Y.; Wu, H.; Hatzistergos, M.; Hung, P. Y.; Tieckelmann, R.; Tsai, W.; Hobbs, C.; Ye, P. D. Chloride molecular doping technique on 2D materials: WS_2 and MoS_2. *Nano Lett.* **2014**, *14*, 6275−6280.

(19) Keldysh, L. V. Diagram technique for nonequilibrium processes. *Sov. Phys. JETP* **1965**, *20*, 1018−1026.

(20) Kresse, G.; Furthmüller, J. Efficient iterative schemes for ab initio total-energy calculations using a plane-wave basis set. *Phys. Rev. B* **1996**, *54*, 11169.

(21) Taylor, J.; Guo, H.; Wang, J. Ab initio modeling of open systems: Charge transfer, electron conduction, and molecular switching of a C60 device. *Phys. Rev. B* **2001**, *63*, No. 121104.

(22) Taylor, J.; Guo, H.; Wang, J. Ab initio modeling of quantum transport properties of molecular electronic devices. *Phys. Rev. B* **2001**, *63*, No. 245407.

(23) Waldron, D.; Liu, L.; Guo, H. Ab initio simulation of magnetic tunnel junctions. *Nanotechnology* **2007**, *18*, No. 424026.
(24) The lattice constant of WS_2 monolayer yields the better agreement well with the experimental values,[25] as compared to PBE. Moreover, the splitting of conduction and valence band due to SOC is in agreement with the ARPES results.[34]
(25) Terrones, H.; Lopez-Urias, F.; Terrones, M. Novel hetero-layered materials with tunable direct band gaps by sandwiching different metal disulfides and diselenides. *Sci. Rep.* **2013**, *3*, 1549.
(26) Lu, Z. W.; Singh, D.; Krakauer, H. Equilibrium properties of hcp titanium and zirconium. *Phys. Rev. B* **1987**, *36*, 7335−7341.
(27) Davey, W. P. Precision Measurements of the Lattice Constants of Twelve Common Metals. *Phys. Rev.* **1925**, *25*, 753−761.
(28) Wood, R. M. The Lattice Constants of High Purity Alpha Titanium. *Phys. Soc.* **1962**, *80*, 783.
(29) Huang, X.; Li, F.; Zhou, Q.; Wu, G.; Huang, Y.; Wang, L.; Liu, B.; Cui, T. In situ synchrotron X-ray diffraction with laser-heated diamond anvil cells study of Pt up to 95 GPa and 3150 K. *RSC Adv.* **2015**, *5*, 14603−14609.
(30) Ahmed, Z.; Afzalian, A.; Schram, T.; Jang, D.; Verreck, D.; Smets, Q.; Schuddinck, P.; Chehab, B.; Sutar, S.; Arutchelvan, G. Introducing 2D-FETs in device scaling roadmap using DTCO. In *2020 IEEE International Electron Devices Meeting (IEDM)*; IEEE, 2020; pp. 22.5.1 −22.5.4.
(31) Silvi, B.; Savin, A. Classification of chemical bonds based on topological analysis of electron localization functions. *Nature* **1994**, *371*, 683−686.
(32) Jin, L.; Koester, S. Contact Gating in Dual-Gated WS_2 MOSFETs With Semi-Metallic Bi Contacts. *IEEE Electron Device Lett.* **2022**, *43*, 1575−1578.
(33) Shen, P.-C.; Su, C.; Lin, Y.; Chou, A.-S.; Cheng, C.-C.; Park, J.-H.; Chiu, M.-H.; Lu, A.-Y.; Tang, H.-L.; Tavakoli, M. M.; Pitner, G.; Ji, X.; Cai, Z.; Mao, N.; Wang, J.; Tung, V.; Li, J.; Bokor, J.; Zettl, A.; Wu, C. I.; Palacios, T.; Li, L. J.; Kong, J. Ultralow contact resistance between semimetal and monolayer semiconductors. *Nature* **2021**, *593*, 211−217.
(34) Kastl, C.; Chen, C.; Koch, R.; Schuler, B.; Kuykendall, T.; Bostwick, A.; Jozwiak, C.; Seyller, T.; Rotenberg, E.; Weber-Bargioni, A.; Aloni, S.; Schwartzberg, A. M. Multimodal spectromicroscopy of monolayer WS_2 enabled by ultra-clean van der Waals epitaxy. *2D Mater.* **2018**, *5*, No. 045010.

https://doi.org/10.1021/acsomega.2c08275
ACS Omega 2023, 8, 10419−10425